Hybrid Control of Self-Oscillating Resonant Converters With Three-Level Input

Nicola Zaupa, Carlos Olalla, Isabelle Queinnec, Luis Martínez-Salamero, Luca Zaccarian

Hybrid Control of Self-Oscillating Resonant Converters with Three-Level Input

Nicola Zaupa, Carlos Olalla, Isabelle Queinnec, Luis Martínez-Salamero, Luca Zaccarian

***Abstract*— We propose a hybrid feedback law inducing self-oscillating behavior in second-order resonant converters. With our controller, the converter switches at the resonant frequency of its tank, without the need of external oscillators. In addition, the output amplitude can be adjusted by a reference signal ranging from zero to $\pi/2$. The amplitude modulation is then performed while maintaining an approximately constant switching frequency. Theoretical results show uniqueness and almost global asymptotic stability of a nontrivial hybrid limit cycle. Experimental results show that a circuit implementing the new controller successfully matches the desirable simulated behavior.**

***Index Terms*— Stability of hybrid systems, Lyapunov methods, Power electronics.**

I. Introduction

CONTROL of resonant converters is a well-known problem in power electronics associated with several solutions [1]–[3]. Conventional approaches include frequency modulation, where the switching frequency is the control input [4], [5], and amplitude modulation, where the control input is the phase-shift between the two legs of the switches [6], [7]. Frequency modulation may induce desirable zero voltage switching (ZVS) but the regulation of the operating point may require wide frequency ranges. Conversely, amplitude modulation desirably operates at constant switching frequency, at the expense of losing ZVS.

This paper adopts a state-plane hybrid control approach inducing self-oscillation of the resonant converter without the need of external inputs. State-plane based methods that turn to self-oscillating schemes have been proposed in the past, either ensuring the oscillations regardless of the load condition [7], [8], or proposing state-plane-induced input selection [9], [10]. Our approach has several advantages with respect to these previous papers. First, we relax the conservative requirement imposed by [9], [10] on the quality factor. Secondly, the proposed controller has useful links with the conventional control methods, as explained next.

This work was supported in part by: the Spanish Ministry of Science and Innovation under projects PID2019-111443RB-100 and PID2020-120151RB-I00; the ANR via grant HANDY, number ANR-18-CE40-0010; and the MUR under PRIN grant DOCEAT, number 2020RTWES4.
(*Corresponding author: Nicola Zaupa (e-mail: nzaupa@laas.fr).*)

Nicola Zaupa, Isabelle Queinnec and Luca Zaccarian are with LAAS-CNRS, University of Toulouse, CNRS, Toulouse, France. Luca Zaccarian is also with Università di Trento, 38123 Trento, Italy.

Carlos Olalla and Luis Martínez-Salamero are with the Departament d'Enginyeria Electrònica, Elèctrica i Automàtica, Escola Tècnica Superior d'Enginyeria, Universitat Rovira i Virgili, 43007 Tarragona, Spain.

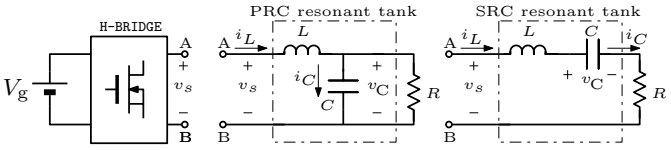

Fig. 1. Parallel resonant converter and series resonant converter.

In our previous works [11], [12], we addressed the control of second-order parallel and series resonant converters (PRC and SRC, respectively) with the hybrid formulation of [13] in a unified way. To represent the switching input voltage v_s of the resonant tank we used there a discrete variable $\sigma \in \{-1, 1\}$. The hybrid control law allowed regulation of the converter by changing the operating frequency. Thus, the hybrid controller provided a self-oscillating *frequency modulation* behavior.

Given the limitations of using wide frequency ranges in resonant conversion, the objective of this paper is to propose and to validate a hybrid controller that allows modulation of the amplitude of the first harmonic of the input voltage v_s. The hybrid controller produces, in a way, a self-oscillating *amplitude modulation* behavior. We introduce here a third value for $\sigma \in \{-1, 0, 1\}$ corresponding to a zero voltage input, allowing us to operate at the resonant frequency of the tank across a range of output amplitudes.

The fact of having a three-level input voltage is beneficial in two ways: modulation of input voltage first harmonic is possible and the harmonic content is reduced. The last point is supported by [14] since PRC and SRC are topologically similar to three-level neutral point clamped inverters (NPC) feeding a lossless LC two-port terminated at a resistive load. On the other hand, NPC requires an external sinusoidal reference tuned at the proper frequency. While, in our three-level input voltage SRC and PRC it is not required because the hybrid control induces an oscillation at the resonant frequency.

The paper is structured as follows. The system model and the proposed controller are discussed in Section II. Section III states and proves our main theoretical result and Section IV reports the experimental implementation and validation on a power converter prototype. Section V conclude the work.

Notation. $\mathbb{R}$ ($\mathbb{R}_{>0}$) [$\mathbb{R}_{\geq 0}$] and $\mathbb{Z}$ ($\mathbb{Z}_{>0}$) [$\mathbb{Z}_{\geq 0}$] are the sets of (positive) [non-negative] real and integer numbers. $\mathbb{R}^n$ denotes the n-dimensional Euclidean space. Given two vectors $u \in \mathbb{R}^n$ and $w \in \mathbb{R}^m$, $u^\top$ denotes the transpose of u, and $(u, w) := \begin{bmatrix} u^\top & w^\top \end{bmatrix}^\top$ denotes their stacking. Given a (continuous, discrete, or hybrid) signal x, $\dot{x}$ denotes its derivative with respect to continuous time t, while x^+ denotes

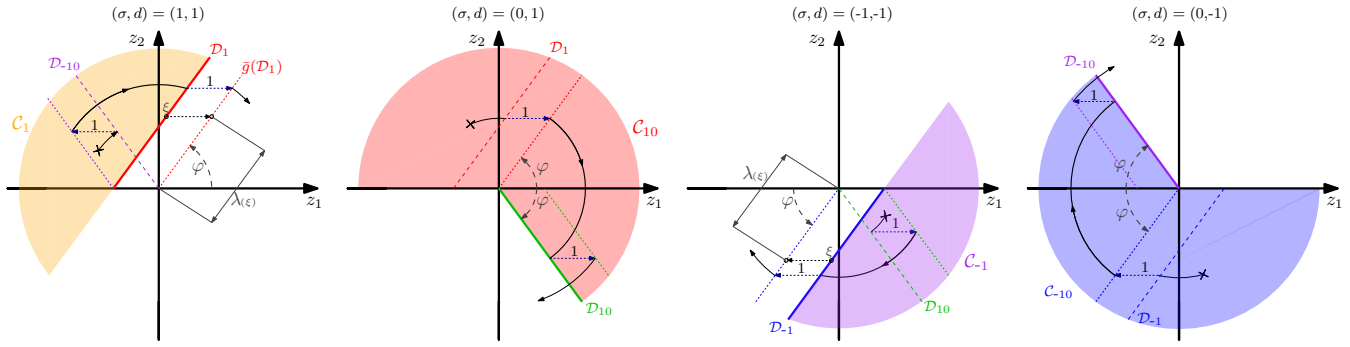

Fig. 2. Jump sets (solid lines) and flow sets (sectors) for each selection of (σ, d). A sample trajectory is represented in black. Coordinate λ will be introduced and used in the proof.

its next value with respect to discrete time j.

II. System Model and Proposed Controller

We address parallel and series second-order resonant converters (PRC and SRC, respectively) as shown in Fig. 1. As in [11], [12], consider the following change of coordinates

$$z_1 := \frac{v_C}{V_g} - \sigma, \quad z_2 := \frac{1}{V_g}\sqrt{\frac{L}{C}}i_C, \tag{1}$$

based on the voltage and current on the capacitor (v_C and i_C) and the discrete variable $\sigma \in \{-1, 0, 1\}$ representing the switching input voltage v_s of the resonant tank, so that $v_s = \sigma V_g$, where V_g is the external DC supply. Following the derivation in [11, eqs. (1) to (4)], the continuous-time dynamics of both converters is unified to

$$\dot{z}_1 = \omega z_2, \quad \dot{z}_2 = -\omega z_1 - \beta z_2, \tag{2}$$

where $\omega := \left(\sqrt{LC}\right)^{-1}$ is the natural frequency and $\beta > 0$ is the inverse of the time constant of the exponential decay associated with each resonant tank of Fig. 1:

$$\beta_{\text{PRC}} := \frac{1}{RC}, \quad \beta_{\text{SRC}} := \frac{R}{L}. \tag{3}$$

This novel approach to control (1) includes the possibility to apply a zero voltage input $\sigma = 0$. While this extra value does not change coordinates (1) nor their continuous dynamics (2), it radically changes the switching possibilities, which are here described by a hybrid model enforcing a precise periodic sequence for σ: 1, 0, -1, 0, ... (in practice σ is a three-level square waveform):

$$\begin{bmatrix}\dot{z}_1\\ \dot{z}_2\\ \dot{\sigma}\\ \dot{d}\end{bmatrix} = f(\xi) = \begin{bmatrix}\omega z_2\\ -\omega z_1 - \beta z_2\\ 0\\ 0\end{bmatrix} \qquad \xi \in \mathcal{C}(\varphi), \tag{4a}$$

$$\begin{bmatrix}z_1^+\\ z_2^+\\ \sigma^+\\ d^+\end{bmatrix} = g(\xi) = \begin{bmatrix}z_1 + d\\ z_2\\ -d + \sigma\\ -d + 2\sigma\end{bmatrix} \qquad \xi \in \mathcal{D}(\varphi). \tag{4b}$$

In our new model (4), $\xi := (z_1, z_2, \sigma, d)$ collects the four states: two physical and two logical ones. The logical state σ denotes the switch position, as in [11], [12]. The new logical state $d \in \{-1, 1\}$ plays an important role when $\sigma = 0$ as it stores the past value of σ, so that the next value will be assigned as the opposite one (i.e. $-d$), in order to generate the correct switching pattern. Clearly, any variation of σ and d must be instantaneous, so that $\dot{\sigma} = 0$ and $\dot{d} = 0$.

The angle $\varphi \in [0, \pi/2)$ is a reference input affecting the steady-state output voltage (minimum for $\varphi = \pi/2$ and maximum for $\varphi = 0$). Based on φ, we select the jump and flow sets as

$$\begin{aligned}\mathcal{C}(\varphi) &:= \mathcal{C}_1(\varphi) \cup \mathcal{C}_{10}(\varphi) \cup \mathcal{C}_{-1}(\varphi) \cup \mathcal{C}_{-10}(\varphi),\\ \mathcal{D}(\varphi) &:= \mathcal{D}_1(\varphi) \cup \mathcal{D}_{10}(\varphi) \cup \mathcal{D}_{-1}(\varphi) \cup \mathcal{D}_{-10}(\varphi),\end{aligned} \tag{5a}$$

which correspond to the union of four jump and flow sets graphically illustrated in Fig. 2. Selection (5a) intuitively leads to a reduced phase mismatch between v_s and i_C, as shown by the sample solution of (4), (5) represented in black. More precisely, for each $q \in \{-1, 1\}$, define

$$\begin{aligned}\mathcal{C}_q(\varphi) := \{(z, \sigma, d) :\ &\sigma = q, d = q,\\ &d\left((z_1 + \sigma)\sin\varphi - z_2\cos\varphi\right) \le 0\},\end{aligned} \tag{5b}$$

$$\begin{aligned}\mathcal{C}_{q0}(\varphi) := \{(z, \sigma, d) :\ &\sigma = 0, d = q,\\ &\left(d\left(z_1\sin\varphi - z_2\cos\varphi\right) \ge 0\right) \vee (dz_2 \ge 0)\},\end{aligned} \tag{5c}$$

$$\begin{aligned}\mathcal{D}_q(\varphi) := \{(z, \sigma, d) :\ &\sigma = q, d = q, dz_2 \ge 0,\\ &(z_1 + \sigma)\sin\varphi - z_2\cos\varphi = 0\},\end{aligned} \tag{5d}$$

$$\begin{aligned}\mathcal{D}_{q0}(\varphi) := \{(z, \sigma, d) :\ &\sigma = 0, d = q, dz_2 \le 0,\\ &z_1\sin\varphi + z_2\cos\varphi = 0\}.\end{aligned} \tag{5e}$$

Note that $\mathcal{D}_1(\varphi)$ and $\mathcal{D}_{-1}(\varphi)$ are horizontally translated with respect to the origin. Therefore, when $\sigma = 0$, solutions flow by spanning a constant cone centered at the origin, so that the flowing interval is constant regardless of the amplitude of z. Secondly, the zero crossing of the current i_C (proportional to z_2) happens approximately at the middle of that flowing interval (the lower β the better this approximation, due to the higher quality factor). This results in keeping v_s and i_C mostly in phase and, for the SRC configuration, it ensures that the input voltage and the current of the resonant tank are almost synchronized.

Remark 1 Shifting horizontally the two jump sets $\mathcal{D}_1$ and $\mathcal{D}_{-1}$ has a desirable effect on the relation between φ and the output amplitude. First, we can reach zero amplitude for $\varphi = \pi/2$. Secondly, the static relation between φ and

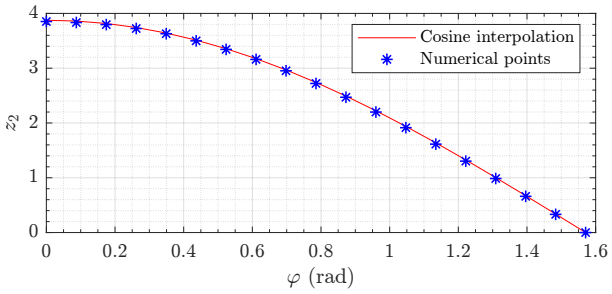

Fig. 3. Amplitude of the first harmonic of z_2 with respect to $\varphi \in [0, \pi/2)$. Interpolating cosine function (red, solid) vs simulations results (blue $\star$).

the steady-state amplitude of z_2 is well interpolated by a cosine function: $A_{ss}(\varphi) = \frac{4}{\pi R}\sqrt{\frac{L}{C}}\cos\varphi$, where $\frac{4}{\pi R}\sqrt{\frac{L}{C}}$ is the amplitude of the first harmonic of i_C normalized by z_2 at the resonant frequency. See Fig. 3, showing simulation results (blue asterisks) vs the graph of the function A_{ss}. ◦

III. Stability of the Resonant Behavior

A. Main result

For our main stability result we require a mild underdamped assumption (see [12, Remark 1]) for the oscillating behavior, requiring that flowing solutions revolve in the phase-plane of Fig. 2, which ensures existence of a non trivial asymptotically stable hybrid limit cycle (as defined in [12] and recalled below) for any reference input $\varphi \in [0, \pi/2)$.

Assumption 1 *The relation $2\omega > \beta > 0$ is satisfied, namely the resonant tank is underdamped. Equivalently, the roots of $s^2 + \beta s + \omega^2 = 0$ are complex conjugate.*

Definition 1 *[12] Given an hybrid system $\mathcal{H} = (\mathcal{C}, f, \mathcal{D}, g)$, a nontrivial* hybrid periodic trajectory *ζ is a complete solution (namely, a solution that evolves forever) that is not identically zero and for which there exists a pair $(T, J) \in \mathbb{R}_{\geq 0} \times \mathbb{Z}_{\geq 0}$ satisfying $T + J > 0$, such that $(t, j) \in \mathrm{dom}(\zeta)$ implies $(t + T, j + J) \in \mathrm{dom}(\zeta)$ and, moreover,*

$$\zeta(t, j) = \zeta(t + T, j + J). \tag{6}$$

The image of ζ is a nontrivial hybrid periodic orbit.

We state next the main theoretical result of this work. It states the asymptotic stability of a nontrivial hybrid periodic orbit with basin of attraction corresponding to the whole space except for the four points (see the green dots in Fig. 4) in the set $\mathcal{K} := \{(0, 0, 0, -1), (0, 0, 0, 1), (-1, 0, 1, 1), (1, 0, -1, -1)\}$. These points comprise weak equilibria[1] and they do not belong to the basin of attraction: for example, solutions starting from $(0, 0, 0, -1)$ and $(0, 0, 0, 1)$ can flow forever staying there or may jump to $(-1, 0, 1, 1)$ or $(1, 0, -1, -1)$ and then: either flow and converge to the hybrid limit cycle, or continue to jump among the points in $\mathcal{K}$.

[1]A weak equilibrium is a point from which there exist constant solutions but also non-constant ones.

Theorem 1 *Under Assumption 1, for each selection of $\varphi \in [0, \pi/2)$, the closed loop (4), (5) has a unique nontrivial hybrid periodic orbit $\mathcal{O}_\varphi$ that is stable and almost globally attractive with basin of attraction $\Xi = (\mathbb{R}^2 \times \{-1, 0, 1\} \times \{-1, 1\}) \setminus \mathcal{K}$.*

B. Preliminary observations to prove Theorem 1

Let us define the set $\Omega = \Omega_1 + \Omega_{-1} + \Omega_{10} + \Omega_{-10}$ as the set of points visited by any solution flowing in $\mathcal{C}$ from $g(\mathcal{D})$. More rigorously, denoting $t \mapsto \psi_{\xi_0}(t, 0)$ any flowing solution of (4) from ξ_0, for each $i \in \{1, -1, 10, -10\}$, we define

$$\Omega_i = \{\xi \in \mathcal{C} : \xi = \psi_{g(\xi_0)}(t, 0) \text{ for some } \xi \in \mathcal{D}_i, t \geq 0\}.$$

Sets Ω_1 and Ω_{-1} correspond to two cones centered at the origin. Set Ω_{10} (resp. Ω_{-10}) corresponds to a cone minus an area limited by what we may call *boundary solution*, which flows from the cone vertex $z_v = (1, 0)$ (resp. $z_v = (-1, 0)$). About this *boundary solution*, it is well defined for any $\varphi \in [0, \pi/2)$ since the vector field at the vertex is vertical, therefore the solution is forced to initially flow inside the cone and then, due to Assumption 1, it revolves clockwise while flowing, until it reaches $\mathcal{D}_{-1}$ (resp. $\mathcal{D}_1$). We define the scalar $\lambda_m > 0$ as the distance between the vertex $(1, 0)$ (resp. $(-1, 0)$) and the point where the *boundary solution* intersects $\mathcal{D}_{-1}$ (resp. $\mathcal{D}_1$) after flowing in the cone.

Fig. 4 depicts λ_m, the set Ω, the set $\mathcal{P} := (\mathcal{D}_1 \cup \mathcal{D}_{-1}) \cap \Omega$, and the coordinate $\lambda \in [\lambda_m, +\infty)$ defined as

$$\lambda = \Lambda(\xi) := \left|\left[\begin{smallmatrix} 1 & 0 & 0 & 0 \\ 0 & 1 & 0 & 0 \end{smallmatrix}\right] g(\xi)\right|, \quad \forall \xi \in \mathcal{P}, \tag{7}$$

see also the first and third diagram in Fig. 2.

The following lemma is an immediate property of solutions and is stated without proof.

Lemma 1 *Set Ω is forward invariant and all solutions from Ω are unique. Moreover, all solutions from $(\mathcal{C} \cup \mathcal{D}) \setminus \mathcal{K}$ converge to Ω in uniform finite time.*

Introduce now the function $\phi_{\mathcal{P}}(\xi_0) : \Omega \to \mathcal{P}$ returning the value $\psi_{\xi_0}(t_{\mathcal{P}}, j_{\mathcal{P}}) \in \mathcal{P}$, where ψ_{ξ_0} is the solution to (4) starting at ξ_0 (unique by Lemma 1), and $(t_{\mathcal{P}}, j_{\mathcal{P}})$ is

$$(t_{\mathcal{P}}, j_{\mathcal{P}}) = \underset{(t,j) \in \mathrm{dom}\, \psi_{\xi_0}}{\mathrm{argmin}} \; (t + j) \quad \text{s.t. } \psi_{\xi_0}(t, j) \in \mathcal{P}. \tag{8}$$

Intuitively speaking, for any $\xi_0 \in \Omega$, $\phi_{\mathcal{P}}(\xi_0)$ denotes the value of the unique solution starting at ξ_0 the first time that it belongs to $\mathcal{P}$.

C. Proof of Theorem 1

We first prove existence and global asymptotic stability (GAS) from Ω of a hybrid periodic orbit $\mathcal{O}_\varphi$ contained in the interior of Ω, based on a Poincaré analysis. Then by the uniform convergence established in Lemma 1, the result follows.

After the first jump, all solutions must transit through set $\mathcal{P}$. Therefore, we may define a Poincaré map characterizing a solution half-cycle as $\xi^+ = \phi_{\mathcal{P}}(g(\xi)) \in \mathcal{P}$ for any $\xi \in \mathcal{P}$. Due to the central symmetry of the dynamics, we can also

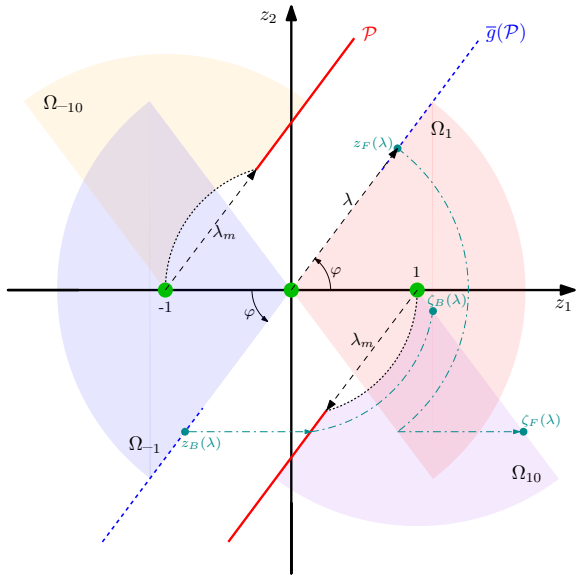

Fig. 4. Projection on the z-plane of the sets: $\boldsymbol{\Omega}$ (shaded areas), $\boldsymbol{\mathcal{P}}$ (solid red lines), $\boldsymbol{\mathcal{K}}$ (green dots) and representation of the *boundary solutions* defining $\boldsymbol{\lambda_m}$ (black dotted arcs). The dashed-dotted lines represent sample solutions used in the proof.

parameterize the Poincaré map in terms of λ, as defined in (7), through description

$$\lambda^+ = \Phi(\lambda), \quad \lambda \in [\lambda_m, +\infty), \tag{9}$$

with $\Phi(\lambda) := \Lambda(\phi_{\mathcal{P}}(\xi_\lambda))$, and $\Lambda^{-1}(\lambda)$ denoting a selection of $\xi_\lambda \in \mathcal{P}$ ensuring $\Lambda(\xi_\lambda) = \lambda$. The discrete dynamics (9) plays the role of a Poincaré map for (4) restricted to Ω. We show below that there exists a unique globally asymptotically stable equilibrium $\lambda^\star = \Phi(\lambda^\star)$ for (9).

Energy function. Due to Lemma 1, we consider next only points $\xi \in \mathcal{P}$. Then, the proof of existence and uniqueness focuses on the behavior of the z components of the unique solution to (4) inducing Φ, in terms of the energy function

$$E(z) := \frac{1}{2}|z|^2. \tag{10}$$

Due to this fact, to simplify our notation, in the sequel, we use $\overline{g}$ to denote the z component of the jump map g. Also, we will employ overlines on the jump and flow sets, to denote their projection on the z plane. With a slight abuse of notation, we will only refer to the z component of the solutions, whenever the σ and d components are clear from the (flow or jump) set under consideration.

Let $\varphi \in [0, \pi/2)$ be fixed and, for each $\lambda \geq \lambda_m$, consider any pair of points $z_F(\lambda) \in \overline{g}(\mathcal{D}_1)$ and $z_B(\lambda) \in \overline{g}(\mathcal{D}_{-1})$ both of them at the same distance λ from the origin, where "F" stands for "Forward" and "B" stands for "Backwards". A pictorial representation of these points and related solutions is shown in Fig. 4. Due to the symmetry of the jump sets, we have $E(z_F(\lambda)) = E(z_B(\lambda)) = \frac{1}{2}\lambda^2$. Consider the points $\zeta_F(\lambda) \in \overline{g}(\mathcal{D}_{10})$ and $\zeta_B(\lambda) \in \overline{g}(\mathcal{D}_{10})$ obtained, respectively, from the forward flowing solution (unique from Lemma 1) starting at $z_F(\lambda)$ and the backward solution starting at $z_B(\lambda)$, jumping back to the unique point $z_B(\lambda)^- \in \mathcal{D}_{-1}$ and then (uniquely) flowing backwards in time in $\mathcal{C}_{-1}$ until they both reach $\overline{g}(\mathcal{D}_{10})$.

Forward solution. About $z_F(\lambda)$ and $\zeta_F(\lambda)$, the forward solution flows in $\mathcal{C}_{10}$ and then jumps after it reaches $\mathcal{D}_{10}$ (which necessarily happens after a finite time, due to the revolving nature of flowing solutions, as induced by Assumption 1). In particular, since $\mathcal{C}_{10}$ is a cone, regardless of λ, the solution flows for a fixed time T and the energy dissipation during such a flowing interval corresponds to $\Sigma_F(\lambda) = \frac{1}{2}\lambda^2(1-\mu(\varphi)^2)$, where $\mu(\varphi)$ (the dependence on φ is dropped in the following) is a constant that can be easily computed from the flowing solution of $\dot{z} = Az$, by solving the equality $\mathrm{e}^{AT}\lambda\left[\begin{smallmatrix}\cos\varphi\\ \sin\varphi\end{smallmatrix}\right] = \lambda\mu\left[\begin{smallmatrix}\cos\varphi\\ -\sin\varphi\end{smallmatrix}\right]$, resulting in $\mu = \left[\begin{smallmatrix}\cos\varphi\\ -\sin\varphi\end{smallmatrix}\right]^\top \mathrm{e}^{AT}\left[\begin{smallmatrix}\cos\varphi\\ \sin\varphi\end{smallmatrix}\right] \in (0,1]$. After this flowing interval, the solution belongs to $\mathcal{D}_{10}$ and must jump (from $\mathrm{e}^{AT}z_F(\lambda) = \lambda\mu\left[\begin{smallmatrix}\cos\varphi\\ -\sin\varphi\end{smallmatrix}\right]$ to $\zeta_F(\lambda)$). This jump is associated with an increase δ_F of the energy E, amounting to

$$\delta_F(\lambda) = \frac{1}{2}\left(|(e^{AT}z_F)^+|^2 - |e^{AT}z_F|^2\right) = \frac{1}{2} + \lambda\mu\cos\varphi. \tag{11}$$

Overall, we may characterize the energy at point $\zeta_F(\lambda)$ as

$$E_F(\lambda) := E(\zeta_F(\lambda)) = \frac{1}{2}\lambda^2 - \Sigma_F(\lambda) + \delta_F(\lambda). \tag{12}$$

Backward solution. Consider now $z_B(\lambda)$ and $\zeta_B(\lambda)$, and also here notice that the backward solution of interest jumps backwards to a point in $\mathcal{D}_{-1}$ denoted as $z_B(\lambda)^- = \lambda\left[\begin{smallmatrix}-\cos\varphi\\ -\sin\varphi\end{smallmatrix}\right] + \left[\begin{smallmatrix}1\\ 0\end{smallmatrix}\right] = \left[\begin{smallmatrix}1-\lambda\cos\varphi\\ -\lambda\sin\varphi\end{smallmatrix}\right]$. The variation of energy across this backward time jump corresponds to

$$\delta_B(\lambda) = \frac{1}{2}\left(|z_B(\lambda)^-|^2 - |z_B(\lambda)|^2\right) = \frac{1}{2} - \lambda\cos\varphi. \tag{13}$$

Continuing in the backwards motion of this solution, for any $\lambda \geq \lambda_m$, we see a flowing interval in the set $\mathcal{C}_{-1}$ where the solution reaches (in finite backwards time) the set $\overline{g}(\mathcal{D}_{10})$, due to the revolving properties induced by Assumption 1.

Applying [12, Lemma 2] such a flowing interval is associated with an energy increase (in backwards time) corresponding to $\Sigma_B(\lambda) := \frac{\beta}{\omega}\Pi(z_B(\lambda)^-)$, where $\Pi(z_B(\lambda)^-)$ is the (unsigned) area hatched between the graph of the backwards trajectory and the axis $z_2 = 0$. Note that Σ_B is a positive and quadratically increasing function of λ.

Overall, we may characterize the energy at point $\zeta_B(\lambda)$ as

$$E_B(\lambda) := E(\zeta_B(\lambda)) = \frac{1}{2}\lambda^2 + \Sigma_B(\lambda) + \delta_B(\lambda). \tag{14}$$

Energy balance. Consider the mismatch function

$$\widetilde{E}(\lambda) := E_F(\lambda) - E_B(\lambda) = \delta(\lambda) - \Sigma(\lambda), \tag{15}$$

where Σ is a quadratically increasing function of λ (it is strongly convex):

$$\Sigma(\lambda) := \Sigma_B(\lambda) + \Sigma_F(\lambda) = \Sigma_B(\lambda) + \frac{1}{2}\lambda^2(1-\mu^2), \tag{16}$$

and δ is a linearly increasing function of λ:

$$\delta(\lambda) := \delta_F(\lambda) - \delta_B(\lambda) = \lambda(1+\mu)\cos\varphi. \tag{17}$$

Lemma 2 *There exist a unique value $\lambda^\star > \lambda_m$ such that $\widetilde{E}(\lambda^\star) = 0$. Moreover, $\lambda^\star$ is a fixed point for Φ in* (9).

Proof: Let us show that $\widetilde{E}(\lambda_m) = \delta(\lambda_m) - \Sigma(\lambda_m) > 0$, which from (15) is equivalent to showing that $E_F(\lambda_m) - E_B(\lambda_m) > 0$. For $\lambda = \lambda_m$, a) the forward solution reaches $\zeta_F(\lambda_m)$ with energy $E_F(\lambda_m) = \frac{1}{2} + \frac{1}{2}\lambda_m^2\mu^2 + \lambda_m\mu\cos\varphi$; b) by definition of λ_m, the backward solution reaches the vertex $\zeta_B = (1,0)$ with energy $E_B(\lambda_m) = \frac{1}{2}$. Therefore $E_F(\lambda_m) - E_B(\lambda_m) = \frac{1}{2}\lambda_m^2\mu^2 + \lambda_m\mu\cos\varphi$, which is the sum of two positive scalars. Since function $\lambda \mapsto \widetilde{\psi}(\lambda) := -\widetilde{E}(\lambda)$ is negative at λ_m and strongly convex, then, from [12, Lemma 1], there exists a unique positive value $\lambda^\star > \lambda_m$ such that $\widetilde{E}(\lambda^\star) = 0$. Finally, we can express the energy difference, in terms of λ, between the final and initial points $\Phi(\lambda)$ and λ, as $\widetilde{E}(\lambda) = \frac{1}{2}(\Phi(\lambda)^2 - \lambda^2)$. From which we conclude that $\lambda^\star$ is a fixed point for (9). ■

The corresponding points $\xi^\star \in \mathcal{P}$ that satisfy $\Lambda(\xi^\star) = \lambda^\star$, and the image of the unique solution originating from those points is a unique nontrivial hybrid periodic orbit in the interior of Ω (because $\lambda^\star > \lambda_m$), characterized as

$$\mathcal{O}_\varphi = \{\xi \in \Omega : \ \Lambda(\phi_{\mathcal{P}}(\xi)) = \lambda^\star\}. \tag{18}$$

Lyapunov function.

In order to prove GAS of the hybrid periodic orbit we reduce the stability analysis to the Poincaré map (9). We have already shown that there exists a unique equilibrium point $\lambda^\star = \Phi(\lambda^\star)$. Then, we introduce the quadratic Poincaré-like Lyapunov function,

$$V(\lambda) := (\lambda - \lambda^\star)^2. \tag{19}$$

Similar to the final part of the proof of [15, Lemma 2], to prove global asymptotic stability, we show that:

$$V(\Phi(\lambda)) - V(\lambda) < 0 \quad \forall \lambda \geq \lambda_m, \ \lambda \neq \lambda^\star,$$

or, equivalently,

$$(\Phi(\lambda) - \lambda)(\Phi(\lambda) + \lambda - 2\lambda^\star) < 0 \quad \forall \lambda \geq \lambda_m, \ \lambda \neq \lambda^\star. \tag{20}$$

To show this, let us divide the study for $\lambda > \lambda^\star$ and $\lambda < \lambda^\star$. From the proof of Lemma 2, for $\lambda > \lambda^\star$, we have that $\widetilde{E}(\lambda) < 0$, which implies $\Phi(\lambda) - \lambda < 0$, in other terms $\lambda > \Phi(\lambda) > \lambda^\star$ where $\Phi(\lambda) > \lambda^\star$ comes from the uniqueness of flowing solutions so that they cannot cross. Next, we assess the positivity of the second term in (20) as $\Phi(\lambda) + \lambda - 2\lambda^\star > 2(\Phi(\lambda) - \lambda^\star) > 0$. For the case $\lambda < \lambda^\star$, similar considerations hold, leading to (20). Finally, continuity of Φ follows from similar reasonings to [15, Lemma 2] and the stability of $\lambda^\star$ for (9) proved above, imply global asymptotic stability of $\mathcal{O}_\varphi$ in (18) from Ω, following the steps in [15, Proposition 1], which are here omitted due to length restrictions. Finally, GAS of $\mathcal{O}_\varphi$ from Ξ follows from the uniform convergence established in Lemma 1.

IV. Experimental Validation

The results of Theorem 1 are validated on an experimental SRC prototype and via simulations. The experimental setup consists in an SRC designed for a 50 kHz resonant frequency. The DC power supply is $V_g = 24\,\text{V}$, the resonant tank components are $L = 94.5\,\mu\text{H}$ and $C = 100\,\text{nF}$. The control law is implemented in an FPGA where we use ADCs to sense the current and the voltage on the capacitor (needed to compute (z_1, z_2) as illustrated in [11]).

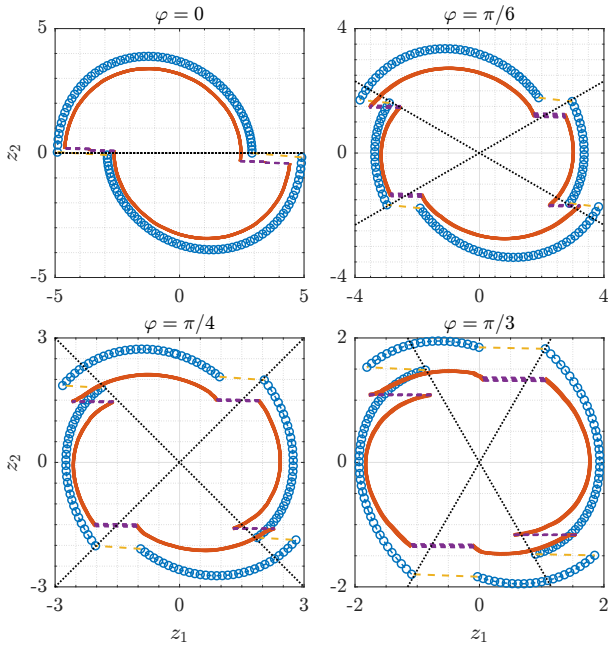

Fig. 5. Phase portraits in the (z_1, z_2) coordinates: simulations (blue circles) and experiments (orange solid line) with different values of φ. The φ-tilted dotted black lines represents the jumps sets. The load is $R = 10.1\,\Omega$.

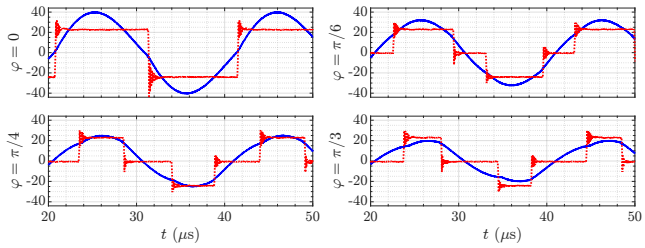

Fig. 6. Input current ($\times$**15** A) (blue line) and input voltage v_s (V) (red line) from the experimental prototype for the values of φ shown in Fig. 5.

The control law is implemented in the FPGA as an automaton with four states, corresponding to the four parts in which one period can be decomposed, based on the variables σ and d: $(\sigma, d) \in \{(1,1),(0,1),(-1,-1),(0,-1)\}$. (see Fig. 2). The jump sets are modeled as half-planes to ensure robustness and simplicity in the implementation. The automaton is allowed to go to the next sequential state whenever 1) jump signal is active and 2) the automaton is in the preceding state (e.g $(\sigma, d) = (1,1)$ and $\mathcal{D}_1$ active: $(z_1 + 1)\sin\varphi - z_2\cos\varphi \geq 0$). Differently from [12], to evaluate the jump conditions, a generic scaled version of (z_1, z_2) is not enough: we need to know the scaling factor in the acquisition chain and compensate for it. This is due to the sets $\mathcal{D}_1$ and D_{-1} being shifted with respect to the origin.

Multiple experiments have been run for two load selections: $R = 10.1\,\Omega$ and $R = 21.8\,\Omega$. Fig. 5 compares the simulated and experimental steady-state responses for different values of φ. We emphasize that no startup controller is needed due to the (almost) global attractivity established in Theorem 1, thus the device starting at rest effectively spirals out to reach the pre-

scribed oscillating behavior. The corresponding experimental time waveforms are reported in Fig. 6. Note that, the input current (i.e. the capacitor current, due to the SRC configuration) is approximately in phase with the input voltage. Having the first harmonics aligned implies improved performance in terms of efficiency, since more power is transmitted to the load and less power is dissipated in the resonant tank. Finally, Figs. 7 and 8 compare the simulated and experimental frequencies and amplitudes. The black horizontal dotted lines show the resonant frequencies evaluated by characterizing the resonant tank, with the load, at low power. The physical controller presents some limits for low amplitudes (large φ) due to the resolution of the ADCs and the amplitude of the noise. Therefore, only a subset of values for φ has been validated experimentally.

The experiments confirm the simulation results. The frequency mismatch visible in both figures amounts to an acceptable 4%. Minor amplitude discrepancies are also visible, probably due to model uncertainties (e.g. nonlinear dependence of the inductor on the current, parasitic effect on the PCB, sampling effects) but the reliable closed-loop behavior illustrates the robustness of the proposed control.

V. Conclusions and Future Work

We have proposed a novel state-plane control approach modulating the first harmonic of the input voltage as an emergent self-oscillating behavior: an amplitude modulation approach. Through a reference input $\varphi \in [0, \pi/2)$ we can control the amplitude of the converter output and we can always generate a self-oscillating hybrid limit cycle in underdamped conditions. The expected theoretical and simulated response has been confirmed by experiments on an SRC prototype.

The proposed hybrid controller opens interesting possibilities for future research. First, it can be anticipated that using the reference input for regulation of the converter will present advantageous dynamic properties. Secondly, novel conditions on the hybrid control law ensuring zero voltage switching would reduce the switching losses and open new possibilities on operating the power converters at their best efficiency points.

References

[1] R. Erickson and M. Dragan, *Fundamentals of Power Electronics*, 3rd ed. Springer Nature, 2020.

[2] R. Oruganti and F. C. Lee, "Resonant Power Processors, Part II-Methods of Control," *IEEE Trans. on Industry Applications*, 1985.

[3] M. Youssef and P. Jain, "A review and performance evaluation of control techniques in resonant converters," in *30th Annual Conference of IEEE Industrial Electronics Society, 2004. IECON 2004*, 2004.

[4] V. Vorperian, "Approximate small-signal analysis of the series and the parallel resonant converters," *IEEE Tran. on Power Electronics*, 1989.

[5] Y. Yin, R. Zane, J. Glaser, and R. Erickson, "Small-signal analysis of frequency-controlled electronic ballasts," *IEEE Transactions on Circuits and Systems I: Fundamental Theory and Applications*, 2003.

[6] J. Burdio, F. Canales, P. Barbosa, and F. Lee, "Comparison study of fixed-frequency control strategies for ZVS DC/DC series resonant converters," in *IEEE Power Electronics Specialists Conference*, 2001.

[7] M. Youssef, H. Pinheiro, and P. Jain, "Self-sustained phase-shift modulated resonant converters: Modeling, design, and performance," *IEEE Transactions on Power Electronics*, 2006.

[8] H. Pinheiro, P. Jain, and G. Joos, "Performance characterization of two self-oscillating controllers for parallel resonant converters operating with unity input power factor," in *Record 28th Annual IEEE Power Electronics Specialists Conference*, 1997.

[9] R. Bonache-Samaniego, C. Olalla, L. Martínez-Salamero, and H. Valderrama-Blavi, "Design of self-oscillating resonant converters based on a variable structure systems approach," *IET Power Electronics*, 2016.

[10] R. Bonache-Samaniego, C. Olalla, and L. Martínez-Salamero, "Dynamic Modeling and Control of Self-Oscillating Parallel Resonant Converters Based on a Variable Structure Systems Approach," *IEEE Transactions on Power Electronics*, 2017.

[11] N. Zaupa, L. Martínez-Salamero, C. Olalla, and L. Zaccarian, "Results on hybrid control of self-oscillating resonant converters," in *IFAC Conference on Analysis and Design of Hybrid Systems*, Jul. 2021.

[12] N. Zaupa, L. Martínez-Salamero, C. Olalla, and L. Zaccarian, "Hybrid control of self-oscillating resonant converters," *IEEE Transactions on Control Systems Technology*, pp. 1–8, 2022.

[13] R. Goebel, R. Sanfelice, and A. Teel, *Hybrid Dynamical Systems: modeling, stability, and robustness*. Princeton University Press, 2012.

[14] A. Nabae, I. Takahashi, and H. Akagi, "A New Neutral-Point-Clamped PWM Inverter," vol. IA-17, no. 5, pp. 518–523, 1981.

[15] A. Bisoffi, F. Forni, M. Da Lio, and L. Zaccarian, "Relay-based hybrid control of minimal-order mechanical systems with applications," *Automatica*, vol. 97, pp. 104–114, 2018.

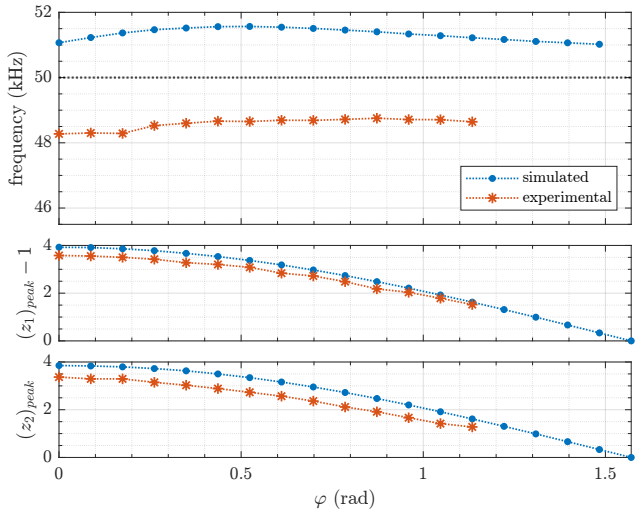

Fig. 7. Simulated and experimental responses with $\boldsymbol{R} = 10.1\,\Omega$. The black dotted line is the estimated resonant frequency $\hat{\boldsymbol{f}}_{\boldsymbol{0}} = 50\,\text{kHz}$.

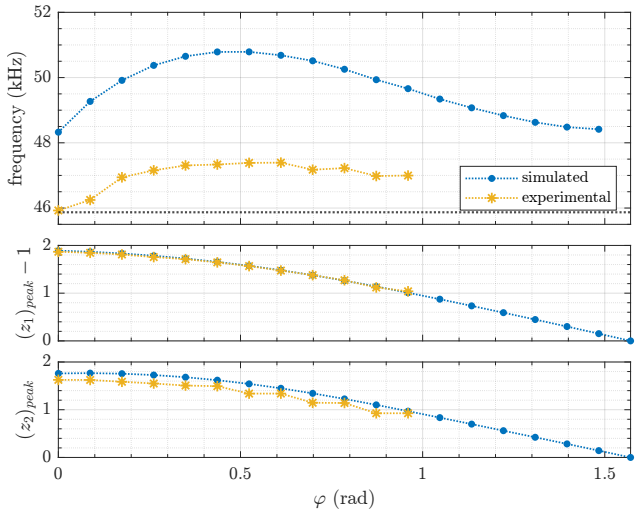

Fig. 8. Simulated and experimental responses with $\boldsymbol{R} = 21.8\,\Omega$. The black dotted line is the estimated resonant frequency $\hat{\boldsymbol{f}}_{\boldsymbol{0}} = 45.8\,\text{kHz}$.